Editors' Suggestion | Featured in Physics

Nanoscale Transport during Liquid Film Thinning Inhibits Bubble Coalescing Behavior in Electrolyte Solutions

Bo Liu,[1,2] Rogerio Manica,[1] Qingxia Liu,[1,3,*] Zhenghe Xu,[1,4] Evert Klaseboer,[5] and Qiang Yang[2]
[1]Department of Chemical and Materials Engineering, University of Alberta, Edmonton,T6G 1H9, Canada
[2]School of Mechanical and Power Engineering, East China University of Science and Technology, Shanghai 200237, China
[3]Julong college, Shenzhen Technology University, Shenzhen 518118, China
[4]Department of Materials Science and Engineering, Southern University of Science and Technology, Shenzhen, 518055, China
[5]Institute of High Performance Computing, 1 Fusionopolis Way, Singapore 138632

(Received 23 November 2022; revised 4 February 2023; accepted 21 July 2023; published 8 September 2023)

The long-standing puzzle of why two colliding bubbles in an electrolyte solution do not coalesce immediately upon contact is resolved. The water film between the bubbles needs to be drained out first before its rupture, i.e., coalescence. Experiments reveal clearly that the film thinning exhibits a rather sudden slowdown (around 30–50 nm), which is orders of magnitude smaller than similar experiments involving surfactants. A critical step in explaining this phenomenon is to realize that the solute concentration is different in bulk and at the surface. During thinning, this will generate an electrolyte concentration difference in film solution along the interacting region, which in turn causes a Marangoni stress to resist film thinning. We develop a film drainage model that explains the experimentally observed phenomena well. The underlying physical mechanism, that confused the scientific community for decades, is now finally revealed.

DOI: 10.1103/PhysRevLett.131.104003

Collision and coalescence of air bubbles in electrolyte solutions are widely encountered in nature and engineering [1–4]. The dissolved electrolytes tend to prevent the bubbles from coalescing quickly, evidenced by the formation of oceanic whitecaps that are rarely observed in rivers and lakes [1,2,5]. Because of its impact on bubble size and residence time in water, this coalescence inhibition effect of electrolytes might be crucial for global climate by affecting sea-air gas flux and aerosol formation [1–3]. It also plays a significant role on heat and mass transfer in bubble-related engineering processes such as vaccine production, mineral extraction, and water splitting [6–9].

Over the past five decades, numerous studies have been conducted to exploit the coalescence inhibition effect of electrolytes [10–14], but little is known about the underlying physical mechanism [12,14]. The established theories for surfactants to prevent bubble coalescence, which emphasize the surfactant absorption onto the air-water surfaces, are not applicable because many electrolytes (e.g., NaCl) are depleted from the surface rather than absorbed onto it [15]. Neither can this be explained by the colloidal stability theory, since electrolytes are widely reported to destabilize the dispersed systems by depressing the repulsive electrical double layer force [16]. A similar coalescence inhibition phenomenon is also found with many non-surface-active solutes such as sucrose, and with electrolytes in nonaqueous solutions [11,17]. These unexplained findings collectively suggest that there might be undiscovered physics related to this liquid-gas bubbling system.

When two bubbles collide in a liquid, they deform, and a very thin liquid film forms between them on the micrometer scale [14,16,18,19]. The impact of electrolytes on bubble coalescence, either by affecting the hydrodynamic liquid flow or the colloidal forces, is expected to manifest itself on the film drainage process [12,13,20]. However, direct information of the film thinning process was limited to quasistatic bubble collision conditions. The absence of thin film experimental information between fast colliding bubbles (e.g., 50 μm/s and above [13]) has greatly hindered the understanding of the electrolytes induced coalescence inhibition effect. In this work, we overcome this limitation by adopting a high-speed interferometry method that directly observes the thin film as a function of space and time between two fast colliding bubbles, and perform a set of controlled experiments to get an in-depth understanding.

In our experiments, two bubbles submerged in an electrolyte solution were brought together to study their collision and coalescence [Fig. 1(a)]. An upper bubble (radius $R_b = 1.00$ mm, generated and held at a capillary orifice) was driven toward a lower bubble (radius R_s between 0.10 and 0.80 mm, immobilized on a transparent hydrophobic silica surface with a contact angle ~100°) at a controlled velocity of 3 mm/s, unless specified otherwise. A light beam was sent in through an inverted microscope. The reflections from both bubble surfaces interfered with each other, changing the light intensity that was recorded by a high-speed camera at 86 400 frames per second. By analyzing the light intensity, we were able to extract the

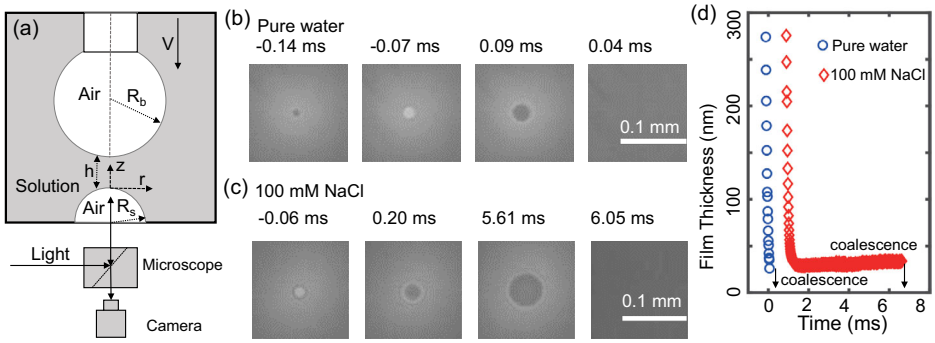

FIG. 1. (a) A sketch of the experimental setup. A bubble of radius $R_b = 1.00$ mm was held at the glass capillary orifice, whereas another bubble of radius R_s was immobilized on a hydrophobic silica surface. The capillary was driven downward with velocity V by a speaker diaphragm to allow bubble collision. A high-speed camera connected to an inverted microscope was used to record the interference fringes. Snapshots of the fringes in a time sequence obtained between two colliding bubbles in (b) pure water ($R_s = 0.41$ mm) and (c) 100 mM NaCl solutions ($R_s = 0.42$ mm). By analyzing the interferometric images, (d) the film thickness evolution was obtained; NaCl curves were shifted by 1 ms for clarity. The difference in film thinning behavior between pure water and water with electrolytes is clearly visible.

spatiotemporal evolution of the film thickness h between two bubbles with nanometer resolution (see Supplemental Material for details [21]).

Figures 1(b) and 1(c) show the evolution of interferometric fringes between two colliding bubbles, and Fig. 1(d) illustrates the extracted film thickness at the film center in pure water and 100 mM NaCl solution, respectively. For comparison, we define "$t = 0$" as the time when the surfaces would have touched if they were nondeformable (e.g., rigid spheres), thereby setting a reference time to measure how long film rupture was delayed (termed "coalescence time"). In pure water, the film thinned with negligible delay that enabled almost instantaneous coalescence ($t = 0.14$ ms), indicating that the air-water surfaces had fully tangential mobile surface boundary conditions, a feature that was recently confirmed using the same technique [19]. In stark contrast, a two-stage film thinning behavior was observed for a 100 mM NaCl solution. At the initial stage, the film thinning was almost identical to that of pure water, featured by a small film width and rapid light intensity evolution. When the film thickness reached around 30 nm, the rapid thinning was suddenly "arrested," accompanied by the expansion of the black film [Fig. 1(c)], thereby delaying bubble coalescence to 6.05 ms. The coalescence time t_c can vary by several orders of magnitude with NaCl concentration and bubble size [Fig. 2(a)], whilst the two-stage film thinning process, where the film thinning was "arrested" at the thickness of around 30–50 nm, was consistently observed in the experiments.

The two-stage film thinning behavior, featuring the sudden slowdown at around 30–50 nm, is not limited to NaCl but a general feature in other electrolyte solutions [Fig. 2(b)]. However, the ability to influence the coalescence time varied significantly with the type of electrolyte. For example, it requires 50 mM $CaCl_2$, 1000 mM HNO_3, and 1500 mM $NaClO_4$ [see Fig. 2(c)] to achieve a similar coalescence time as for 100 mM NaCl. This relationship agrees with the findings that the coalescence inhibition ability of different electrolytes follows a reverse order for these electrolytes to affect, either decrease or increase, the air-water surface tension [10].

The above experimental observation marks a critical step in understanding the impact of electrolytes on bubble coalescence. The delayed coalescence time of milliseconds is of the same order as the time for bubbles to interact in a

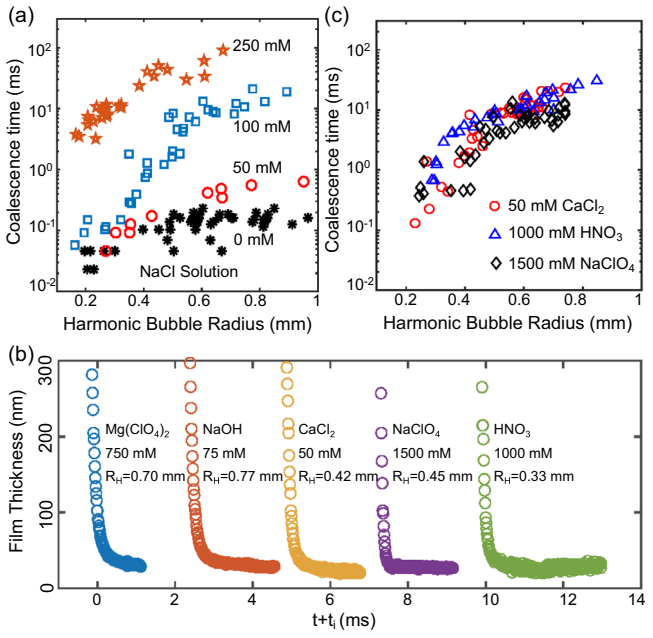

FIG. 2. (a) Coalescence time as a function of harmonic mean radius $R_H = 2R_sR_b/(R_s + R_b)$, in NaCl solutions at different concentrations. (b) Two-stage film thinning behavior until bubble coalescence is observed in different electrolyte solutions; each curve has been shifted by a time t_i for clarity. (c) Variation of coalescence time with R_H in different electrolyte solutions.

typical bulk situation (estimated to be around 0.01–0.12 s [33]). The variations of t_c with bubble size, electrolyte concentration, and type agree well with the literature reported data on coalescence probability, i.e., a longer t_c would contribute to a lower coalescence probability [4,10,12]. Therefore, we can conclude that electrolytes affect bubble coalescence by delaying the film thinning at the film thickness of ~30–50 nm for milliseconds, an interesting behavior that has not been observed previously. It remains a challenge though to address the question of why electrolytes delay film rupture at such a small film thickness. In comparison, surfactants are shown to delay the film thinning at a much larger thickness of a few microns and on a longer timescale of seconds [19]. Surface forces, such as the repulsive electrical double layer force, affect the film thinning at a similar thickness of tens of nanometers. However, they should stabilize the film for a much longer time of minutes rather than just a few milliseconds [14,16,19]. Therefore, the well-established theories for surfactants to inhibit bubble coalescence, by affecting the hydrodynamic flow and surface forces, are not applicable to electrolytes.

A Gibbs elasticity model proposed by Marrucci predicts a two-stage film thinning behavior and identifies the importance of bubble size, electrolyte concentration, and electrolyte type on coalescence time [10,20,34]. However, the model predicts a film thinning behavior that clearly deviates from the experimental observation. In the Gibbs elasticity model, the thin liquid film was assumed to be stretched as a whole, like "a rubber sheet being pulled at the periphery" [20], such that there is no mass transfer between the film and the bulk. Using this assumption, the film expansion is expected to occur at the rapid film thinning process but stop at the deceleration stage, just in a reverse order compared with our experimental observations that the film expansion does not start until the film thinning is arrested. Furthermore, the Gibbs elasticity model cannot explain the coalescence inhibition effect for a mixture of electrolytes [12]. Inspired by the key physical insight of the Gibbs elasticity model that the film thinning can be delayed by the surface tension gradient induced by the electrolyte concentration gradient in the solution, we developed an electrolyte transport model to reveal the underlying physics.

When developing the electrolyte transport model, a critical consideration is the surface-bulk partition of electrolytes [15,28,29,35], which enables a different electrolyte concentration at the surface compared with the bulk. More precisely, some electrolytes are depleted [e.g., NaCl, as sketched in Fig. 3(ii)] whereas some others (e.g., $HClO_4$) are accumulated at the surface region [15,28,29]. The surface concentration can be quantified using the Gibbs definition of surface excess $\Gamma = -[C/RT(1+\epsilon_{\pm})](d\sigma/dC)$, where R is the ideal gas constant, T is temperature, C is the electrolyte concentration of the film solution, $\epsilon_{\pm}$ is a nonideality correction term that varies with electrolyte type, and σ is

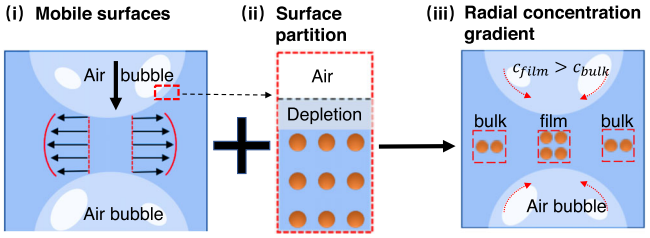

FIG. 3. Schematics for the electrolyte transportation process within the thin liquid film for surface depleted electrolytes (e.g., NaCl). With (i) the mobile surfaces and (ii) the surface depletion behavior, (iii) electrolyte concentration inside the film region starts to rise, enabling a radial electrolyte concentration gradient, hence a surface tension gradient that reduces the surface mobility.

the surface tension [10,36]. The quantity $d\sigma/dC$ can be approximated as a constant only dependent on electrolyte type (see Fig. S3 [21]). The approximate linear relationship between Γ and C is described as $\Gamma = 0.5 h_{\text{salt}} C$, where $h_{\text{salt}} = -2[1/RT(1+\epsilon_{\pm})](d\sigma/dC)$ is a constant, and the factor 2 describes the contribution from both bubbles. In the film thinning process, the electrolytes flow out simultaneously inside the film solution and through the surface because of the intrinsically mobile air-water interface. The role of surface transport, at a different concentration from the film solution, becomes non-negligible in the highly confined thin liquid film.

By summing the transport of electrolyte through the surface and the film solution together and making certain simplifications (see the detailed mathematical formulation and discussion in the Supplemental Material [21]), the electrolyte transport equation is written as

$$\frac{DC}{Dt} = -\frac{h_{\text{salt}}}{(h+h_{\text{salt}})}\frac{C}{h}\frac{Dh}{Dt}. \tag{1}$$

In Eq. (1), $D/Dt = \partial/\partial t + U\partial/\partial r$ is the material derivative, r is the radial coordinate, U is surface velocity, and h_{salt} is the unit of length that is typically within ±2 nm. When $h \gg h_{\text{salt}}$, the right-hand side of Eq. (1) is so small that $DC/Dt \approx 0$, suggesting a negligible change of electrolyte concentration C within the interaction region. When h reduces to the small thickness of 30–50 nm, the right-hand side can no longer be neglected, i.e., $DC/Dt \neq 0$. The solution concentration C at the interaction area starts to vary to form a concentration gradient in the radial direction, hence a Marangoni stress that slows down the film thinning [see Fig. 3(iii)]:

$$\frac{\partial h}{\partial t} = -\frac{1}{r}\frac{\partial}{\partial r}(rUh) + \frac{1}{12\mu_w r}\frac{\partial}{\partial r}\left(rh^3\frac{\partial p}{\partial r}\right) \tag{2}$$

$$\frac{\sigma}{2r}\frac{\partial}{\partial r}\left(r\frac{\partial h}{\partial r}\right) = \frac{2\sigma}{R_H} - (p+\Pi). \tag{3}$$

Starting with an initial concentration $C = C_0$, Eq. (1) is solved numerically coupled with Eq. (2) to describe the

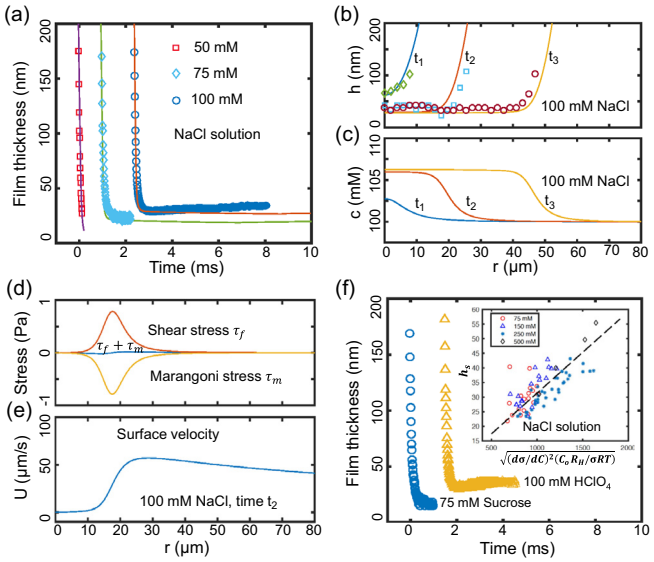

FIG. 4. (a) Comparison between theory (lines) and experimental observations (symbols) of the center film thickness evolution. Three concentrations are included: $C_0 = 50$ mM, $R_s = 0.19$ mm, $C_0 = 75$ mM, $R_s = 0.42$ mm, $C_0 = 100$ mM, $R_s = 0.42$ mm; curves are shifted for clarity. (b) The lateral film thickness at three times ($t_1 = -0.01$ ms, $t_2 = 1.13$ ms, $t_3 = 4.59$ ms) in 100 mM NaCl solution, $R_s = 0.47$ mm. (c) The NaCl concentration distribution within the thin liquid film. At time t_2, (d) the fluid shear stress and Marangoni stress distribution and (e) the surface velocity distribution within the thin liquid film. (f) The film thinning behavior until bubble coalescence in sucrose solution with $R_s = 0.43$ mm, and in $HClO_4$ solution with $R_s = 0.49$ mm; curves are shifted for clarity. The inset shows a linear relationship between the measured h_s and $\sqrt{(d\sigma/dC)^2(C_o R_H/\sigma RT)}$, with varying C_0 and R_H in experiment.

lubrication flow inside the thin film with the solution viscosity μ_w [19,30], and Eq. (3) (Young-Laplace equation) to illustrate the surface deformation under the hydrodynamic pressure p and disjoining pressure Π [16,19]. The formation of an electrolyte concentration gradient in the radial direction $\partial C/\partial r$, as predicted by Eq. (1), results in a surface tension gradient $\partial\sigma/\partial r$ that affects the surface velocity U in Eq. (2). This impact is achieved by balancing the stresses at the interface $\tau_b = \partial\sigma/\partial r + \tau_f$, where τ_f and τ_b are the shear stress exerted on the interface by the liquid flow inside the film and the airflow inside the bubbles, respectively. The complete theoretical model is provided in the Supplemental Material [21]. Without any fitting parameters, a notable agreement between model predictions and experimental results is shown in Fig. 4(a). The key features in the experimental observation, e.g., the rapid film thinning at the initial stage and the slowdown behavior at a thickness of tens of nanometers are all quantitatively predicted by the newly developed theoretical model. The flattening of the curved bubble surfaces and the expansion of the thin film area are also successfully captured by the model [see Fig. 4(b)]. The bubbles start to deform-flatten when the hydrodynamic pressure becomes closer to the bubble Laplace pressure ($2\sigma/R_H$). At the initial stage with almost fully mobile air-water interfaces, the hydrodynamic pressure is negligible, contributing to a small film width. Once the surface mobility is reduced dramatically, the hydrodynamic pressure starts to build up to deform the bubbles and contributes to the film expansion. Agreement between theory and experiment validates the model performance on predicting the film thickness evolution, the transition of boundary conditions, and the pressure distribution.

With the validated model, we can now gain a deeper insight into what occurs within the thin liquid film during its thinning process. In 100 mM NaCl, the bulk concentration shows negligible variation compared with the initial concentration until the film is thinned to ~50 nm [see Fig. 4(c)]. Afterward, the electrolyte concentration rises and reaches a peak of ~105 mM accompanied by the film expansion. With the small variation (~5%) of electrolyte concentration, a surface tension difference of around 10^{-5} N/m is formed along the transition region of ~10 μm, giving rise to the Marangoni stress $d\sigma/dr$ of ~1 Pa that was sufficient to counterbalance the fluid shear stress τ_f [Fig. 4(d)]. The overall stress profile enabled a surface velocity close to zero at the flattened region, but much larger in the curved region [see Fig. 4(e)].

The model also applies to surface-enriching electrolytes like $HClO_4$, where film electrolyte concentration decreases as surfaces approach, but once again contributes to an inward Marangoni stress that resists film thinning because $d\sigma/dC < 0$ (see supporting video in the Supplemental Material [21]). Furthermore, the theory presented here can be extended to electrolyte mixtures (see Fig. S7 and the subsequent discussion in the Supplemental Material [21]) exhibiting an additive effect [12,31], and may be transposed to other systems with non-surface-active solutes as the two-stage film thinning behavior is also observed in the sucrose-in-water solution [see Fig. 4(f)].

The thickness at which the film flattened h_s is the most important parameter that determines the measured coalescence time. Reducing this value by a few nanometers allows the film to be ruptured by the attractive Van der Waals force, as observed in 50 mM NaCl solution. A simplified scaling analysis of the developed model links h_s with experimental properties as $h_s \sim \sqrt{(d\sigma/dC)^2(C_0 R_H/\sigma RT)}$. This relationship agrees well with the experimental data [Fig. 4(f) inset] and clearly highlights the key parameters affecting coalescence time: initial electrolyte concentration C_0, electrolyte type through $d\sigma/dC$, and bubble size R_H. The impact of other critical parameters, such as collision velocity and solution viscosity [37,38], should expressed through Eq. (2).

We can also interpret the empirical cation-anion pair relationship on bubble coalescence, which has been extensively discussed for decades [4,11,12], within the same theoretical framework by linking it to $d\sigma/dC$. For

electrolytes, $d\sigma/dC$ is determined by the quantitative surface-bulk partition of electrolytes [15,28,29], which is not only affected by ion-specific properties such as hydration and polarization, but also determined by the counterions through electrostatic interaction [15,29,35]. Therefore, $d\sigma/dC$ is strongly affected by the pairing of cation and anion. This indicates that the cation-anion relationship has the same physical origin as the Hofmeister series on protein precipitation, although the latter focuses more on the direct ion-surface interaction [15,39] rather than the quantitative distribution of electrolytes. Interestingly, the effect of coions and the solute additivity are attracting increasing attention in recent research of ion-specific Hofmeister effects [32,40].

In summary, we demonstrate that electrolytes prevent bubble coalescence by abruptly decelerating film thinning at a thickness of around 30–50 nm. This abnormal thinning feature is explained quantitatively by a theory incorporating the transport of electrolytes, both in the film solution and at the surface, into the film drainage process. The thus generated electrolyte concentration difference in the film solution causes Marangoni stresses on the bubble surface that renders the surface effectively immobile and delays the film drainage. The in-depth understanding resolves the long-standing puzzle and may facilitate the control of bubbles widely encountered in nature and engineering, e.g., reducing the bubble-related energy loss in electrochemical systems [8,9]. Moreover, the developed theory may serve as a framework for studying surfactant-like coalescence inhibition behavior in various surfactant-free systems.

We are thankful for the suggestions from Professor John Ralston (University of South Australia), Professor Ming Gong (Fudan University, China), Professor Honglai Liu (ECUST, China), Dr. Adrien Bussonniere (CNRS, France), Dr. Jing Chang (XUST, China), and Mr. Hanrui Zheng. We acknowledge the financial support of the Natural Science and Engineering Research Council of Canada. Bo Liu, Qiang Yang, and Qingxia Liu acknowledge the financial support from National Natural Science Foundation of China under Grants No. 22178099, No. 52025103, and No. 52174255, and the Shenzhen Key Laboratory of Marine Energies and Environmental Safety under Grant No. ZDSYS20201215154000001. B. L. is sponsored by the Shanghai Pujiang program. Author contribution: B. L., R. M., Q. L., and Z. X. designed the research; B. L. performed the research; B. L. and R. M. analyzed the data and developed the model; Q. Y. provided suggestions on reframing the structure and improved the scaling analysis, E. K. helped with the theoretical modeling; B. L. wrote the manuscript; and all authors commented on it.

*qingxia2@ualberta.ca

[1] G. B. Deane and M. D. Stokes, Nature (London) **418**, 839 (2002).
[2] H. Czerski, Phys. World **30**, 34 (2017).
[3] J. C. Bird, R. De Ruiter, L. Courbin, and H. A. Stone, Nature (London) **465**, 759 (2010).
[4] V. S. Craig, B. W. Ninham, and R. M. Pashley, Nature (London) **364**, 317 (1993).
[5] Y. Katsir, G. Goldstein, and A. Marmur, Colloids Interface Sci. Commun. **6**, 9 (2015).
[6] T. A. Grein, D. Loewe, H. Dieken, T. Weidner, D. Salzig, and P. Czermak, Front. Bioeng. Biotechnol. **7**, 78 (2019).
[7] R.-H. Yoon, Miner. Eng. **6**, 619 (1993).
[8] A. Angulo, P. van der Linde, H. Gardeniers, M. Modestino, and D. F. Rivas, Joule **4**, 555 (2020).
[9] P. Lv, P. Peñas, H. LeThe, J. Eijkel, A. vandenBerg, X. Zhang, and D. Lohse, Phys. Rev. Lett. **127**, 235501 (2021).
[10] G. Marrucci and L. Nicodemo, Chem. Eng. Sci. **22**, 1257 (1967).
[11] V. S. Craig, B. W. Ninham, and R. M. Pashley, J. Phys. Chem. **97**, 10192 (1993).
[12] V. S. Craig, Curr. Opin. Colloid Interface Sci. **16**, 597 (2011).
[13] Y. Katsir and A. Marmur, Langmuir **30**, 13823 (2014).
[14] R. G. Horn, L. A. Del Castillo, and S. Ohnishi, Adv. Colloid Interface Sci. **168**, 85 (2011).
[15] Y. Levin, A. P. dos Santos, and A. Diehl, Phys. Rev. Lett. **103**, 257802 (2009).
[16] D. Y. C. Chan, E. Klaseboer, and R. Manica, Soft Matter **7**, 2235 (2011).
[17] C. L. Henry and V. S. Craig, Langmuir **24**, 7979 (2008).
[18] B. Liu, R. Manica, X. Zhang, A. Bussonnière, Z. Xu, G. Xie, and Q. Liu, Langmuir **34**, 11667 (2018).
[19] B. Liu, R. Manica, Q. Liu, E. Klaseboer, Z. Xu, and G. Xie, Phys. Rev. Lett. **122**, 194501 (2019).
[20] G. Marrucci, Chem. Eng. Sci. **24**, 975 (1969).
[21] See Supplemental Material at http://link.aps.org/supplemental/10.1103/PhysRevLett.131.104003 for details on bubble generation, interferometry method, model derivation, and an introduction, as well as two movies, showing (1) experimental observation on the film thinning behavior between two colliding bubbles and (2) theoretical modeling of the film thinning behavior, which includes Refs. [4,15,18,19,16,22–32].
[22] S. Abid and A. Chesters, Int. J. Multiphase Flow **20**, 613 (1994).
[23] I. U. Vakarelski, R. Manica, X. Tang, S. J. O'Shea, G. W. Stevens, F. Grieser, R. R. Dagastine, and D. Y. Chan, Proc. Natl. Acad. Sci. U.S.A. **107**, 11177 (2010).
[24] D. S. Valkovska and K. D. Danov, J. Colloid Interface Sci. **223**, 314 (2000).
[25] C. L. Henry, C. N. Dalton, L. Scruton, and V. S. Craig, J. Phys. Chem. C **111**, 1015 (2007).
[26] V. Venkateshwaran, S. Vembanur, and S. Garde, Proc. Natl. Acad. Sci. U.S.A. **111**, 8729 (2014).
[27] P. Jungwirth and D. J. Tobias, Chem. Rev. **106**, 1259 (2006).
[28] A. P. dos Santos, A. Diehl, and Y. Levin, Langmuir **26**, 10778 (2010).
[29] L. M. Pegram and M. T. Record, Proc. Natl. Acad. Sci. U.S.A. **103**, 14278 (2006).
[30] R. H. Davis, J. A. Schonberg, and J. M. Rallison, Phys. Fluids A **1**, 77 (1989).
[31] T. T. Duignan, J. Colloid Interface Sci. **600**, 338 (2021).
[32] P. Jungwirth and P. S. Cremer, Nat. Chem. **6**, 261 (2014).

[33] R. Kirkpatrick and M. Lockett, Chem. Eng. Sci. **29**, 2363 (1974).
[34] M. J. Prince and H. W. Blanch, AIChE J. **36**, 1425 (1990).
[35] L. Onsager and N. N. Samaras, J. Chem. Phys. **2**, 528 (1934).
[36] P. K. Weissenborn and R. J. Pugh, J. Colloid Interface Sci. **184**, 550 (1996).
[37] S. Orvalho, P. Stanovsky, and M. C. Ruzicka, Chem. Eng. J. (Lausanne) **406**, 125926 (2021).
[38] S. C. Ozan and H. A. Jakobsen, Int. J. Multiphase Flow **119**, 223 (2019).
[39] L. M. Pegram and M. T. Record, J. Phys. Chem. B **111**, 5411 (2007).
[40] E. E. Bruce and N. F. van der Vegt, J. Am. Chem. Soc. **141**, 12948 (2019).